Optical probing of the minigap in InAs/GaSb superlattices

A. J. L. Poulter, M. Lakrimi, R. J. Nicholas, N. J. Mason, and P. J. Walker
Clarendon Laboratory, University of Oxford, Parks Road, Oxford, OX1 3PU, United Kingdom
(Received 29 October 1998; revised manuscript received 5 March 1999)

We report strong modulations in the far infrared absorption of InAs/GaSb semimetallic superlattices under the influence of a parallel magnetic field and attribute this to direct transitions across the minigap. The experiments have been performed on a variety of structures with the measured minigap energies in the range 3–23 meV. For narrow layered samples where the two band picture is valid a broad minigap absorption is observed. On increasing the well and barrier widths the absorption decreases in energy and also becomes more localized as more bands anticross to form multiple minigaps. The results are compared with parallel field magnetoresistance experiments as well as eight band $\mathbf{k}\cdot\mathbf{p}$ theory. [S0163-1829(99)01527-1]

I. INTRODUCTION

Theoretical predictions made over 15 years ago concerning the nature of so called ''semimetallic'' InAs/GaSb (Refs. 1 and 2) heterostructures by Altarelli[3] have recently been confirmed experimentally by separate groups.[4,5] The controversy has centred on wide layered heterostructures where the negative band gap at $\mathbf{k}=0$ (Γ point) implies semimetallic behavior. However, Altarelli showed using three band $\mathbf{k}\cdot\mathbf{p}$ theory that mixing of the conduction and valence bands at finite k parallel causes a small anticrossing or minigap to be formed close to k_F.[6] $\mathbf{K}\cdot\mathbf{p}$ (Ref. 7) and bond orbital[8] calculations have predicted that the energy gap is of the order of a few meV, and for a purely intrinsic system large changes in behavior should occur, with semiconducting properties expected at low temperatures. In the recent experimental observations, no direct measurement of the minigap energy was possible but its presence was inferred by using parallel magnetic fields to shift the electron and hole dispersion relationships, thus destroying the gap. The capacitance-voltage measurements carried out by Yang *et al.*[4] showed that the system undergoes a transition from a semiconductor at low parallel fields to a semimetal at the point where the magnetic field has decoupled the electron and hole bands, but were unable to determine a value for the minigap energy. Lakrimi *et al.*[5] showed existence of the minigap using temperature-dependent magnetoresistance measurements, again using parallel field to decouple the bands. This latter set of measurements gave a minigap energy of ~7 meV, through modelling of the results using a two band model. Further evidence for the existence of the minigap has also been reported using a double gated configuration,[9] with a measured minigap energy of ~2 meV determined using temperature dependence.

In this paper we present observations of interband transitions across the minigap. Magneto-optical experiments have been performed on a series of semimetallic InAs/GaSb superlattices to study the dependence of the far infrared absorption on parallel magnetic field. The parallel field is used to switch off the interband absorption by inducing a transition to an indirect band structure. The use of parallel magnetic field to induce shifts in the relative positions in k space, for carriers separated in real space, has been used frequently in the past.[10] In this study the same technique is employed so as to cause a relative shift in k parallel between the electron and hole Fermi surfaces of magnitude

$$\Delta k_x = \frac{eBd}{\hbar}, \tag{1}$$

where d is the separation between the electrons and holes, and B is the magnetic field orientated parallel to the y axis. Using a simple two band model[5] (including only the ground electron and heavy hole bands) we have calculated the electron and hole dispersions at finite magnetic field, accounting for the relative shift in k parallel [Eq. (1)]. The calculations show that the anticrossing between the electron and hole bands at finite $k_\parallel$ is shifted and becomes anisotropic in magnetic field (Fig. 1). At low parallel fields the position of the minigap moves relative to the Fermi energy, which can lead to an increase of the absorption across the minigap. On increasing the field further, the transitions at the minigap are blocked by either depopulation of the initial states or population of the final states. At the highest magnetic fields ($B > 10$ T) the bands are completely decoupled, destroying the minigap and producing an indirect gap structure. The far

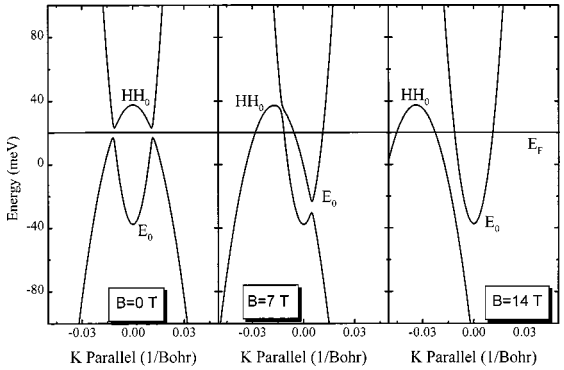

FIG. 1. The effects of the parallel magnetic field induced k space shift on the electron-hole anticrossing. The coupling of the ground electron and hole subbands calculated using a simple parabolic model is shown for field values of 0, 7, and 14 T.

TABLE I. The table shows the layer thicknesses and electron and hole densities per layer for the samples studied. The layer thicknesses are determined by TEM results and growth rules, and the carrier densities are taken from two carrier fits to the Hall data.

Sample	SLS period	Layer width (Å)		Carrier density (10^{11} cm^{-2})	
		InAs	GaSb	Electrons	Holes
OX2029	40	110	100	1.3	1.1
OX1692	20	275	85	4.3	2.3
OX2058	20	220	180	6.9	6.85

infrared interband absorption at the minigap will therefore be extremely dependent on parallel magnetic field.

We report strong absorption (~50%) attributed to interband transitions at the minigap, localized in both energy and magnetic field. The absorption is closely related to parallel field magnetoresistance experiments showing peaks in the resistivity when the Fermi level lies within the minigap. The minigap absorption is studied for a number of samples with varying well and barrier parameters, producing measured minigap energies in the range 3–23 meV depending on the superlattice structure. This large range of minigap energies is compared to theory using an eight band self-consistent $\mathbf{k}\cdot\mathbf{p}$ model.

II. EXPERIMENT

The experiments were performed on a series of 20 and 40 period semimetallic superlattices grown by metal organic vapor phase epitaxy on GaAs substrates, with a GaSb buffer layer of ~2 μm grown before the superlattice to accommodate the strain between the two materials.[11] The carrier densities and mobilities for the samples have been determined by transport measurements using conventional two carrier fits to the Hall data at zero parallel field. The electron and hole gases which are located mainly in the InAs and GaSb layers, respectively, are formed by intrinsic charge transfer between the two layers.[12] There are relatively few external dopants, and the Fermi energy lies close to the miniband gap in the majority of samples studied. For the purposes of this paper we choose to describe just three samples, the details of which are given in Table I, but similar effects have been observed in all samples studied.

Both magneto-optical and magnetoresistance experiments have been performed on the samples in parallel field; however, this paper will concentrate on the optical data with corroboration from the transport measurements, a fuller discussion of which is to be found elsewhere.[5] The optical experiments were performed at a temperature of 2 K using a Bruker Fourier transform (FT) spectrometer. The samples were mounted with the superlattice layers parallel to the magnetic field with the light incident normally onto the sample surface. The transmission was measured using a silicon bolometer mounted out of field center.

As is usual for FT-IR spectroscopy the resulting spectra are complicated due to substrate and background features, and require ratioing to examine the field dependence. In this paper we present two different rationing methods—ratioing the superlattice data against identical measurements performed on a GaSb epilayer (bulk ratio) and, secondly, ratioing the superlattice data against the (superlattice) full field spectrum. The bulk ratio for sample OX1692 is shown in Fig. 2 for a number of different parallel magnetic field values. The large absorption at ~27.5 meV is due to the InAs TO phonon and is not of interest here. The data shows that the transmission of the superlattice in the far infrared (FIR) strongly decreases at lower energies for all magnetic field values. For large magnetic fields (above 8 T) the transmission is seen to be virtually independent of magnetic field over this energy range. At lower magnetic field values however, the low energy transmission (4–12 meV) is seen to depend more strongly on magnetic field, with the observation of a significant absorption centered around 6 meV in the zero field spectrum. At higher energies than this the low field data shows a much smaller magnetic field dependence as seen in the high field case. The absorption at low fields is more clearly seen when the ratio is performed against the full field spectrum. This technique enables us to measure field induced changes in absorption of order 1–2 % at low magnetic fields. Typical examples of the ratioed transmission $T(0)/T(14T)$ are shown (Fig. 3) for the three samples described in detail. The spectra are unreliable below 2.5 meV due to spectrometer limitations, and above 27 meV due to reststrahlen band absorption. The peak feature [Fig. 2(c)] at 16 meV is probably due to a weak field activated hole intersubband absorption present in the 14 T spectrum used for ratioing.

Throughout the paper we will refer to self-consistent eight band $\mathbf{k}\cdot\mathbf{p}$ calculations carried out on the various sample structures. A full discussion of the results of these calculations is given later, but it is found for some of the samples studied here that the ground electron subband lies below more than one hole band at $\mathbf{k}=0$. This means that the simple

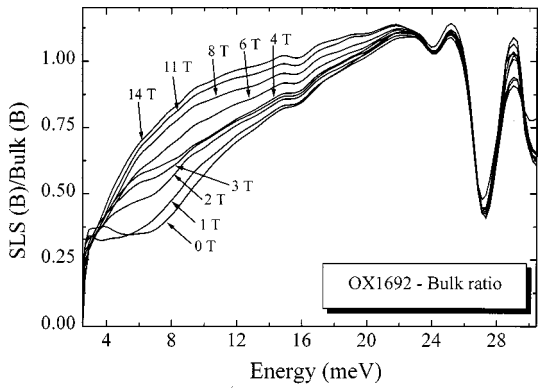

FIG. 2. The transmission spectra for sample OX1692 at various magnetic fields, ratioed against identical measurements performed in parallel magnetic field on a GaSb epilayer.

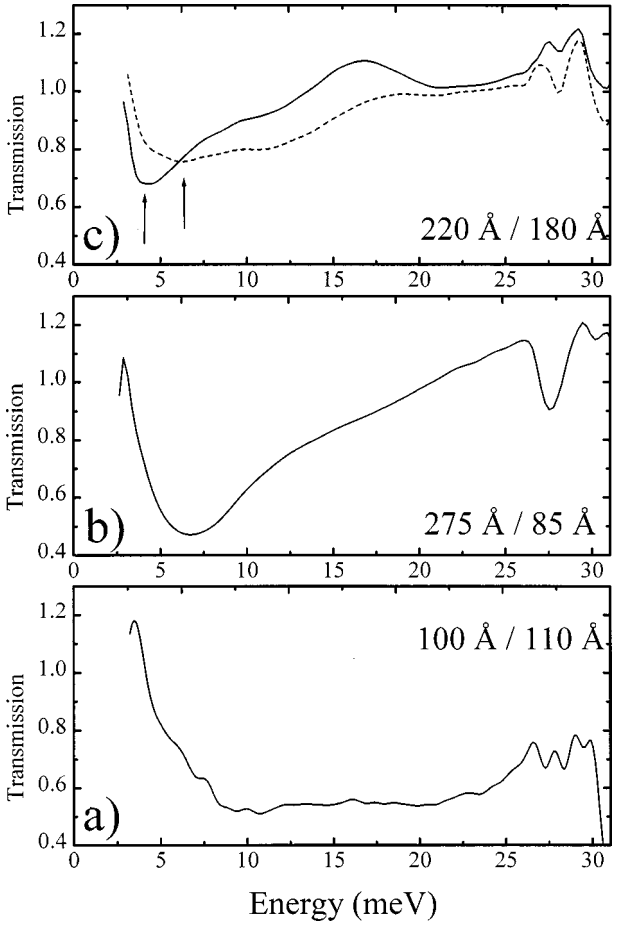

FIG. 3. The transmission spectra at zero magnetic field (ratioed against the full field spectra) are shown for the three samples studied. The caption in each figure denotes the well and barrier widths for the samples. (a) Sample OX2029. (b) Sample OX1691. (c) Sample OX2058. The dotted line represents the trace at 4.5 T (ratioed against the full field spectra). The two arrows indicate the separate minigap absorption features at 0 and 4.5 T.

two band picture often invoked to explain this phenomenon is not valid, and it is necessary to take account of multiple anticrossings between bands in a particular *k*-space direction.

III. RESULTS

The simplest structure studied was sample OX2029 with an InAs (GaSb) width of 110 Å (100 Å). The FIR absorption ratio $T(0)/T(14T)$ is shown in Fig. 3(a), and a broad absorption covering the region of ~8–23 meV can be clearly seen. The spectral information becomes clearer when a series of spectra are taken; the ratioed FIR transmission being measured at constant magnetic field between 0 and 14 T, with field increments of 0.5 T. The optical data is presented in Fig. 4 as a contour map, with maximum absorption of ~50% shown as black. At magnetic fields below 2 T the broad absorption is seen as the dark part of the figure from 8 to 23 meV. At higher fields the absorption reduces steadily as the bands are uncoupled. Figure 4 also shows the parallel field magnetoresistance for the same sample. The sample exhibits a large negative magnetoresistance, the resistivity decreasing by 67% at 14 T compared to the zero field value. In previous work[5,13] we have shown that this rapid decrease is due to the

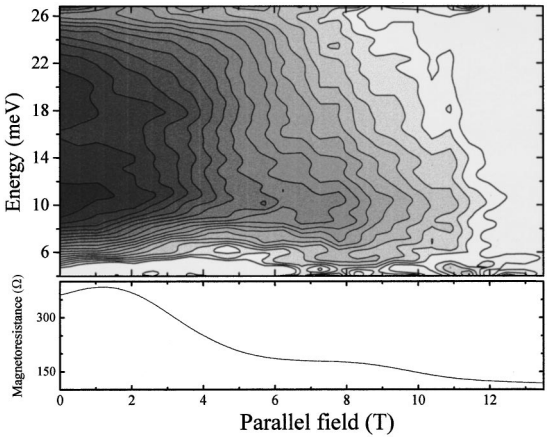

FIG. 4. The optical and transport data for sample OX2029. The optical data was taken at constant magnetic field, with increments of 0.5 T and is shown in the upper half of the figure as a contour plot. The contours vary linearly from 50% absorption (black) to 0% absorption (white) relative to the 14 T trace. The magnetoresistance is shown in the bottom half of the figure. In both cases the *x* axis represents the parallel magnetic field value.

fact that at $B=0$ T the Fermi energy lies close to the minigap, resulting in a large increase of the resistivity, compared with what would be expected for a simple semimetal. When the parallel field is applied, the shifting of the relative positions of the electron and hole dispersion relations removes the minigap causing a large decrease in resistivity. At the magnetic fields at which the resistivity is a maximum, the Fermi level is found to lie within the minigap, which will also enable interband transitions to occur across the gap. A clear correlation is found between the optical and transport data, such that the maximum FIR absorption occurs at magnetic fields below ~2 T when the resistivity is greatest. The disappearance of the absorption occurs once all coupling between the electron and hole states has been removed which is seen by the saturation of the negative magnetoresistance at a field of ~10 T.

The band structure for this sample has been calculated using the eight band $\mathbf{k}\cdot\mathbf{p}$ model, with the *k* parallel dispersion shown at the zone center ($k_z=0$) and also at the superlattice zone boundary ($k_z=\pi/d$) in Fig. 5. The relatively strong quantization of both the electrons and holes removes any complications from the first excited bands (E_1 and HH_1). The calculations show, however, that there is a large dispersion along the superlattice wave vector k_z strongly affecting the magnitude of the minigap. The value of the minigap energy (determined as the minimum energy difference between the two bands) varies from 19.0 meV at $k_z=0$ to 2.9 meV at $k_z=\pi/d$. The theoretical model assumes that the electron and hole bands are isotropic, and if the known valence band anisotropy were included this would undoubtedly increase this dispersion further.[14] From this basic analysis of the band structure we expect an even larger range of minigap energies than observed experimentally (see Fig. 4).

In practice, however, the absorption spectrum is strongly dependent on both the position of the Fermi energy and the interband selection rules for type II structures. For unmixed electron and hole bands, the selection rules for symmetric states that can be assigned a definite parity are found to de-

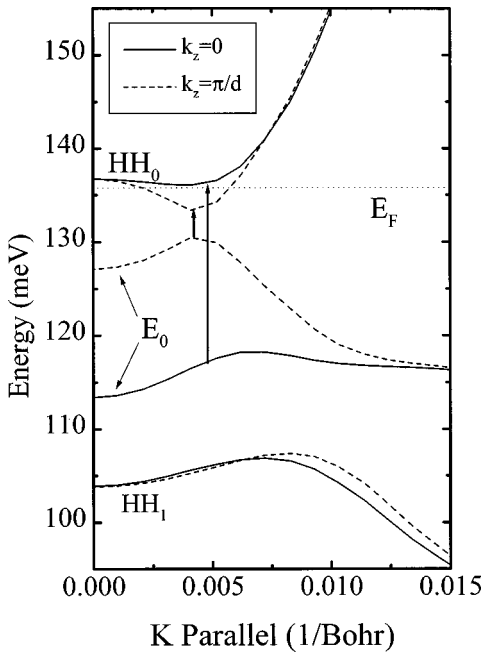

FIG. 5. The calculated band structure for sample OX2029. The solid lines represent the superlattice zone center states ($k_z=0$) and the dashed lines the zone boundary states ($k_z=\pi/d$). The Fermi level is shown as a dotted line. The arrows indicate the energy of the $k_z=0$ and $k_z=\pi/d$ minigaps.

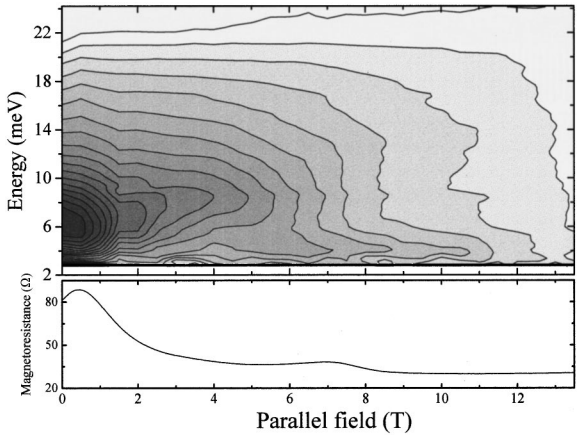

FIG. 6. The optical and transport data for sample OX1692. The optical data was taken at constant magnetic field, at increments of 0.5 T and is shown in the upper half of the figure as a contour plot. The contours vary linearly from 60% absorption (black) to 0% absorption (white) relative to the 14 T trace. The lower half of the figure shows the parallel field magnetoresistance.

pend on both the parity of the states and the superlattice wave vector k_z,[15] as shown in Table II. The selection rules indicate that interband transitions (between E_0 and HH_0) at or close to $k_z=\pi/d$ will be weak; the dominant minigap absorption being closer to the zone center value of 19.0 meV, with a reduced energy dispersion at energies lower than this. The absorption is also influenced by the effects of Fermi level blocking of the final states, particularly close to $k_z=\pi/d$ where the Fermi level rapidly moves through the minigap for small changes in the doping levels of the carriers. Thus the fact that transitions from the superlattice zone edge states (at $k_z=\pi/d$) will be weak, and also that these states are Fermi level blocked for only small changes in the relative concentrations of carriers, results in the low-energy absorption being much reduced. This basic analysis of the band structure shows very clearly the origin of the absorption in the experiment.

The experiments have also been performed on structures with both wider well and barrier widths where the ground electron level at the Γ point ($k_{\|}=0$) lies below more than one hole band. In this case the simple two band picture is no longer valid. We will present measurements on two such structures, the data for the first, sample OX1692 with an InAs (GaSb) width of 275 Å (85 Å), is shown in Figs. 2 and 3(b) and also as a contour plot in Fig. 6. Electrical measurements performed on this sample show that only the ground electron subband is occupied. We observe a much sharper single minigap absorption at magnetic fields below 1.5 T, centered around 6 meV, and with an energy ranging from 4 to 11 meV. The absorption strength relative to the full field value is very strong with a 60% absorption at the minigap. The narrower minigap feature is a characteristic of measurements performed on wider samples where a number of bands anticross close to the minigap, and the k_z dispersion is much reduced. The optical data again agrees well with the parallel field transport measurements, the magnetoresistance decreasing by 63% at full field compared to the zero field value, with a peak in the resistivity corresponding extremely well to the position of maximum absorption in the optical data.

The calculated band structure for this sample is shown in Fig. 7. For the purpose of this discussion the bands are labeled close to $k_{\|}=0$ to avoid confusion as the bands anticross at finite $k_{\|}$. The calculation shows that the ground electron band lies below both HH_0 and HH_1 at the zone center, with a number of anticrossings occurring between the bands. The Fermi level (at zero magnetic field) is found to lie at the anticrossing between the bands labeled HH_0 and HH_1 (at $k_z=0$), with the minigap energy, determined from the minimum separation of these bands, ranging from 4.1 meV ($k_z=\pi/d$) to 9.7 meV($k_z=0$). It is noted that the dispersion

TABLE II. The interband selection rules in a type II structure for symmetric states in a superlattice with equal well and barrier widths. The dependence on the parity of the states and superlattice wave vector k_z are given.

	Transition (E_n-HH_m)	
Superlattice wave vector	n and m same parity	n and m opposite parity
$k_z=0$	allowed	forbidden
$k_z=\pi/d$	forbidden	allowed

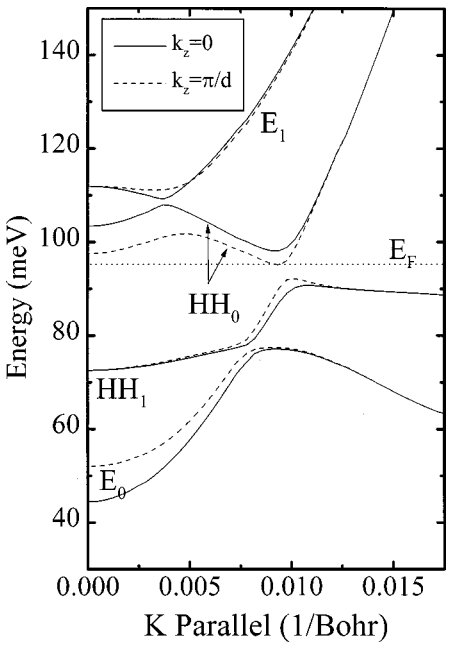

FIG. 7. The calculated band structure for sample OX1692. The solid lines represent the superlattice zone center states ($k_z=0$) and the dashed lines the zone boundary states ($k_z=\pi/d$), with the Fermi level shown as a dotted line. The k dispersion shows the existence of three minigaps although only one occurs at the Fermi level.

along k_z is much reduced for the states at the minigap compared with the thinner sample OX2029, which partly explains the narrower minigap feature observed experimentally in this sample. Careful inspection of the wave functions at the minigap shows that the transition is E_0 to HH_0 in nature. The theoretical minigap energy agrees very well with that observed experimentally, though we do not see any weakening of the absorption of the $k_z=\pi/d$ states as in the previous sample. The absorption at the superlattice zone boundary ($k_z=\pi/d$) will be increased compared to OX2029 due to the large difference in the well and barrier widths causing a breakdown of the k_z selection rules (this is discussed further in the theory section below). We thus expect to observe interband absorption across the entire minigap for this sample, as is confirmed by the comparison between experiment and theory.

The last sample we explore exhibits two separate features in the optical spectra, which is unique for the structures that we have measured. The sample, OX2058 with InAs (GaSb) layer width of 220 Å (180 Å) is found to be intrinsic with the Hall data showing almost equal electron and hole densities. The optical data in Fig. 3(c) and Fig. 8 shows two distinct localized areas of absorption at fields between 0–2 T and 4–5.5 T, with absorption strengths of 33 and 25 %, respectively. The two separate absorptions can be seen more clearly in the 0 and 4.5 T traces (ratioed against the 14 T spectrum) in Fig. 3(c). The minigap feature has narrowed again and its energy has decreased further, ranging from 3–7 meV at low fields and 5–9 meV at higher fields. Figure 8 also shows the transport data, which as well as exhibiting a large negative magnetoresistance shows two peaks, one close to zero field and the second at 4.2 T. The peaks in resistivity correspond closely to the fields at which maximum absorption is found

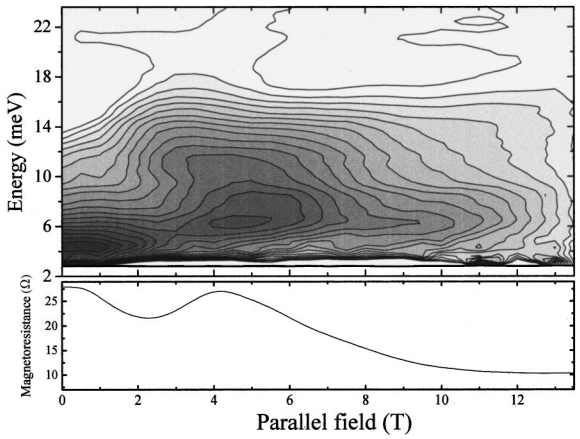

FIG. 8. The optical and transport data for sample OX2058, presented in the same way as Fig. 4. The contours vary linearly from 33% absorption (black) to 0% absorption (white) relative to the 14 T trace. The lower half of the figure shows the parallel field magnetoresistance. Note the existence of a second peak at ~4.5 T in both sets of data.

to occur in the optical measurements. It is thought that the second feature in both sets of data (at ~4.5 T) originates as the Fermi energy passes through the minigap for the second time, at the point where the two Fermi surfaces start to completely decouple. For samples OX2029 and OX1692, a weak feature attributed to the uncrossing of the Fermi surfaces is observed in the transport data at magnetic fields of ~8 and ~7 T, respectively. Careful inspection of the optical data shows a region of absorption at low energies persisting up to higher magnetic fields in these two samples. We suggest that this is also due to transitions across the minigap at the region where the Fermi surfaces decouple. In both samples the energy of this absorption is less than the minigap energy close to zero field and is measured at ~10 and ~4 meV for OX2029 and OX1692, respectively. The decrease in minigap energy at finite field is expected and is explained by the magnetoelectrical hybridization of the states causing a reduction of the interband coupling.

The calculated band structure for sample OX2058 is shown in the region of the Fermi level in Fig. 9. The reduced heterostructure confinement of the holes, compared with the previous two samples, means that five hole bands lie above the ground electron subband at the zone center. Consequently the dispersion relationship at finite k parallel is complicated, with interactions between a number of bands forming the anticrossings close to the Fermi level. We will therefore not assign the observed minigap absorption to transitions between particular bands as in the previous two samples. However, the figure shows that transitions are possible from HH_1 to HH_0 and HH_2 to HH_0 with energies in the range 2 to 4 meV and above 9 meV, respectively. The transition energies are in quantitative agreement with experiment.

IV. THEORY

We now consider in more detail modeling of the minigap absorption using eight band self-consistent $\mathbf{k}\cdot\mathbf{p}$ calculations. The modelling has been performed for $B=0$ T, and in the

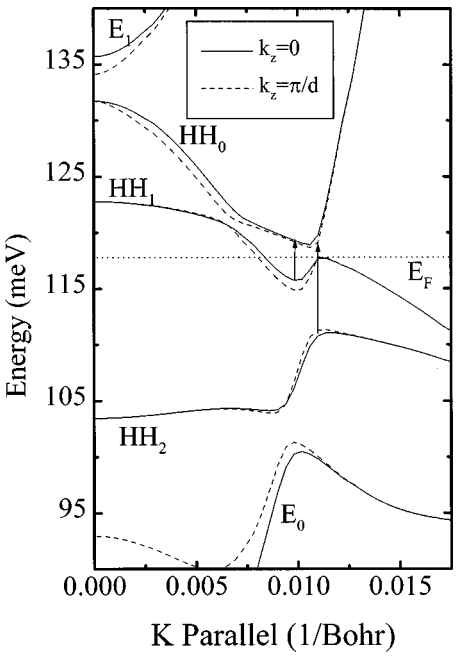

FIG. 9. The calculated band structure for sample OX2058 in the region of energy of the Fermi level. The solid lines represent the superlattice zone center states ($k_z=0$) with the dashed lines representing the zone boundary states ($k_z=\pi/d$). The Fermi level is shown as a dotted line. The arrows indicate possible interband minigap transitions.

comparison with experiments we shall assume that the only effect of the parallel field is to remove the interband minigap absorption due to the decoupling of the bands. This is in complete contrast to the case of intersubband absorption which is extremely weak at $B=0$ T for normal incidence, where we have recently shown that the effect of the parallel field is to strongly enhance the absorption due to additional magnetic confinement and mixing of the in-plane and out of plane motion.[16] The intersubband work has revealed that significant changes to the confinement potential only occurs for samples with wider wells (InAs$>$400 Å) and only at relatively high magnetic fields ($>$10 T). In this case electrons are able to perform cyclotron orbits within a single layer and three-dimensional cyclotron resonances can be observed. We see no evidence of such features in the samples studied here which have thinner layers of InAs.

A number of good reviews of $\mathbf{k}\cdot\mathbf{p}$ theory exist in the literature,[17,18] and only the peculiarities to this system will be discussed here. The broken gap nature of the InAs/GaSb system results in electron-hole coupling occurring not between the electron and hole bands within each particular material but coupling between the electron and hole states in neighboring layers. This, however, can be represented using the $\mathbf{k}\cdot\mathbf{p}$ approach where although separate matrices are constructed for each layer, the boundary conditions—continuity of probability density and current flux across the interface—ensure coupling between states in the separate layers. The calculation is performed by Fourier transforming the Hamiltonian into momentum space creating a ''virtual crystal'' negating the necessity for a transfer matrix approach.[19] This easily accommodates complex and spatially varying potentials, allowing us to perform the calculations self-consistently, taking into account the band bending caused by charge transfer. We have found that this is necessary as the structures studied have densities approaching $1\times10^{12}\,\mathrm{cm}^{-2}$, formed by intrinsic transfer of charge from the GaSb to InAs layers.[1,2,12] In the model we take the InAs-(GaSb) band gap as 418 meV (810 meV), and a band offset of 150 meV between the GaSb valence band and InAs conduction band.

To calculate the optical absorption of the structures we cannot use the simple selection rules presented in Table II due to the strong band mixing of the states close to the minigap. Furthermore the selection rules are only valid for superlattices where the well and barrier widths are equal. This is because the interband transition probability is due to the overlap of the envelope wave functions modulated by the superlattice Bloch condition for the two states. The latter condition gives rise to the k_z dependence of the interband transition probability, and the explicit rules given in Table II for symmetric states in a superlattice with equal well and barrier widths. We have therefore calculated the absorption coefficient in the dipole approximation (in units of absorption per superlattice period per unit illuminated area) and this is given by

$$\alpha(\omega)=\frac{4\pi^2}{nc\omega}\sum_{if}|\langle i|\varepsilon\cdot p|f\rangle|^2\delta(E_f-E_i-\omega)[f(E_i)-f(E_i)],$$

where ω is the frequency, ε the polarization of the incident radiation, n the index of refraction. The summation is over the initial and final states i and f, respectively, with $f(E)$ being the Fermi filling factor of a state at energy E. The first term in the summation is the dipole matrix element which as well as determining the strength of the transition from the wavefunction overlap, also gives rise to the full selection rules.

We will now compare the calculated absorption with the experimental results presented earlier. Due to the small energy of the minigap, the largest uncertainty in comparing theory with experiment is the position of the Fermi level. For small changes in the relative concentrations of the carriers the Fermi level can be moved away from the minigap, blocking minigap transitions. We have therefore performed a series of calculations with p-type and n-type doping to vary the position of the Fermi level relative to the bands. The calculated optical absorption for the OX2029 structure (the band structure shown in Fig. 5) is shown in Fig. 10 for various Fermi level positions, the doping varying from $0.5\times10^{17}\,\mathrm{cm}^{-3}$ (n-type) to $1.5\times10^{17}\,\mathrm{cm}^{-3}$ (p-type). The position of the Fermi level for the intrinsic case ($E_F-E_0=22.3$ meV) is found to lie relatively high in energy (as can be seen in Fig. 5) due to the presence of hole mixing in the electron band. In this case Fermi level blocking of the zone edge ($k_z=\pi/d$) states at $k_\parallel$ values close to the minigap occurs, limiting the low-energy minigap absorption. The calculated absorption coefficient shows a strong peak at 19 meV corresponding to the $k_z=0$ minigap energy, with a much smaller contribution at lower energies. On doping the structure p type the position of the Fermi energy falls, causing depopulation of the $k_z=\pi/dHH_0$ states close to the minigap, enabling interband transitions to occur for all miniband states. The Fermi level is found to lie within the minigap for all k_z values at a p-type doping level of $0.5\times10^{17}\,\mathrm{cm}^{-3}$

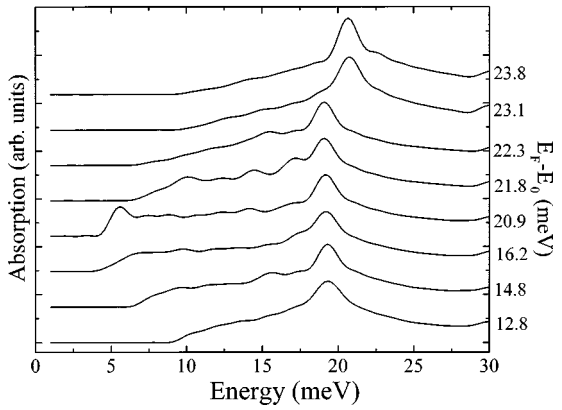

FIG. 10. The calculated optical absorption for sample OX2029 is shown for various doping levels varying from a *n*-type density of $0.5\times10^{17}\,\mathrm{cm}^{-3}$ (top) to a *p*-type density of $1.5\times10^{17}\,\mathrm{cm}^{-3}$ (bottom). The energy of the Fermi level above the E_0 $(k=0)$ state is given on the right of the figure for each trace.

$(E_F-E_0=20.9\,\mathrm{meV})$. We see an increase in the low-energy absorption at this doping level, but a strong peak remains at 19 meV, confirming the selection rules presented in Table II. At higher *p*-type doping levels than this the E_0 subband becomes depopulated for large k_z values, again causing the absorption to shift higher in energy. By doping the well *n* type, the low-energy absorption is further reduced and the peak is shifted to high energies as expected. The calculations show the critical dependence of the absorption on the position of the Fermi energy relative to the minigap. The comparison with experimental results shows that the measured minigap absorption agrees well with the calculations when the Fermi level lies close to the minigap.

The absorption coefficient has also been calculated for the OX1692 structure as is shown in Fig. 11. The calculation is performed with a small amount of *p*-type doping to account for the strong hole mixing in the conduction band, with the

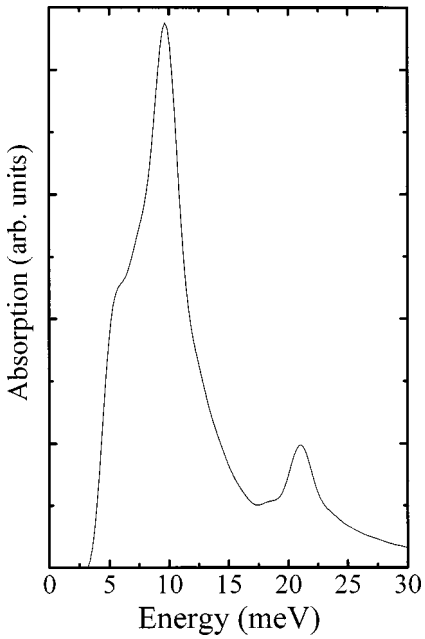

FIG. 11. The calculated optical absorption for sample OX1692, determined from the band structure shown in Fig. 7.

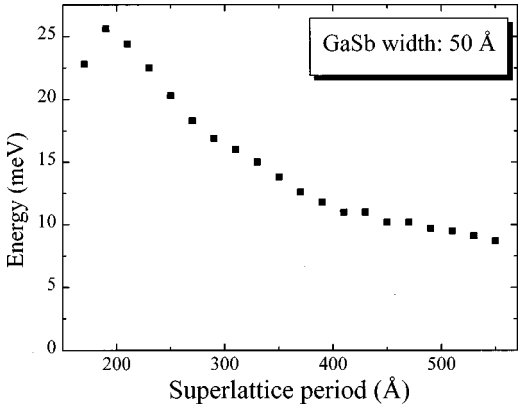

FIG. 12. The variation of the minigap energy with superlattice period is shown for a series of calculations performed on structures with a constant GaSb width of 50 Å, and an InAs width varying from 120 to 500 Å. The points are deduced from the maximum of the absorption.

Fermi level found to lie within the entire minigap (Fig. 7). The absorption shows a strong peak at ~10 meV with significant absorption in the energy range from 5 to 12 meV and a smaller peak at 21 meV. The lower-energy peak agrees well with that observed experimentally, though we do not see any evidence for the higher-energy peak. The calculated absorption exhibits a sharp turn on at low energies showing that the large difference between the well and barrier widths has the effect of reducing the importance of the selection rules at the zone boundary $(k_z=\pi/d)$. Again the strongest absorption is seen above the $k_z=0$ minigap energy (9.7 meV) where the selection rules favor the interband transitions.

We have also performed a series of calculations to investigate the effect of the superlattice period on the minigap energy. The effect of increasing the GaSb layer width is complicated by the presence of a number of hole bands forming multiple anticrossings between the bands. We have therefore performed a series of calculations with a constant GaSb width of 50 Å, which ensures that only the ground hole level lies above the electron bands, with the higher hole bands being strongly confined so as to lie below the ground electron band edge. The results of these calculations are shown in Fig. 12, where the maximum in the calculated absorption is plotted against the superlattice period; the InAs width varying from 120 to 500 Å. The calculations show that the minigap energy depends very much on the interlayer distance, with the coupling energy decreasing strongly on increasing the well width. This is very much as expected as the coupling between conduction and valence band states in adjacent layers will be primarily determined by their separation. At very large InAs well widths the minigap energy decreases more slowly on increasing the InAs well width, and most interestingly the coupling continues to persist. In the widest structures it has been shown experimentally that the effect of the Coulomb potential in wide InAs wells is to split the well into two halves, resulting in a heterojunction at each interface.[20] The coupling in this case will therefore be dominated by electron states bound at the interface, and subsequently the coupling strength will depend less strongly on well width. The slight decrease in the coupling energy for the narrowest structure, is explained by the anticrossing occur-

ring at a smaller k parallel value, due to the small negative band gap between the electron and hole band edge states. As the coupling terms between the electron and heavy hole states are proportional to the k parallel value the minigap energy is therefore reduced. It is noted that the effect at large InAs widths of excited electron subbands becoming occupied and anticrossing with HH_0 is small. For structures with wider GaSb barriers the situation is more complex, but calculations have shown that quantitatively the effect of more than one hole band anticrossing with E_0 is to reduced the minigap energy at the Fermi level.

V. CONCLUSIONS

We have performed magneto-optical and magnetotransport measurements using parallel field to decouple the minigap in InAs/GaSb superlattices. The observed modulations in the far infrared, which agree extremely well with the electrical measurements, have shown that the nature of the minigap is dependent on the superlattice structure both in energy and in the energy dispersion of the minigap. We have presented self-consistent $\mathbf{k}\cdot\mathbf{p}$ calculations to model the structures studied and have found good agreement between theory and experiment. The experimentally observed coupling strength of the electron and hole bands in this material agrees very well with theoretical predictions made in the past using both $\mathbf{k}\cdot\mathbf{p}$ and bond orbital calculations.

ACKNOWLEDGMENTS

This work was financed by EPSRC which we would like to thank for continued support. A.J.L.P. would also like to thank The Technology Partnership PLC (Cambridge, UK) for financial support.

[1] See, for example, L. L. Chang, in *Heterojunctions and Semiconductor Superlattices*, edited by G. Allan, G. Bastard, N. Bocaara, M. Lanno, and M. Voos (Springer, Berlin, 1986), p. 152, and references therein.

[2] E. E. Mendez, L. Esaki, and L. L. Chang, Phys. Rev. Lett. **55**, 2216 (1985).

[3] M. Altarelli, Phys. Rev. B **28**, 842 (1983).

[4] M. J. Yang, C. H. Yang, B. R. Bennett, and B. V. Shanabrook, Phys. Rev. Lett. **78**, 4613 (1997).

[5] M. Lakrimi, S. Khym, R. J. Nicholas, D. M. Symons, F. M. Peeters, N. J. Mason, and P. J. Walker, Phys. Rev. Lett. **79**, 3034 (1997).

[6] J. J. Quinn and J. J. Quinn, Surf. Sci. **361**, 930 (1996).

[7] M. Altarelli, J. C. Maan, L. L. Chang, and L. Esaki, Phys. Rev. B **35**, 9867 (1987).

[8] Y. Naveh and B. Laikhtman, Appl. Phys. Lett. **66**, 1980 (1995).

[9] L. J. Cooper, N. K. Patel, V. Drouot, E. H. Linfield, D. A. Richie, and M. Pepper, Phys. Rev. B **57**, 11 915 (1998).

[10] K. K. Choi, B. F. Levine, N. Jarosik, J. Walker, and R. Malik, Phys. Rev. B **38**, 12 362 (1988).

[11] G. R. Booker, P. C. Klipstein, M. Lakrimi, S. Lyapin, N. J. Mason, R. J. Nicholas, T.-Y. Seong, D. M. Symons, T. A. Vaughan, and P. J. Walker, J. Cryst. Growth **146**, 778 (1994).

[12] D. M. Symons, M. Lakrimi, R. J. Warburton, R. J. Nicholas, N. J. Mason, P. J. Walker, M. I. Eremets, and G. Hill, Phys. Rev. B **49**, 16 614 (1994).

[13] M. Lakrimi, J. Rehman, D. M. Symons, R. J. Nicholas, N. J. Mason, and P. J. Walker, Physica B **258**, 264 (1998).

[14] S. de-Leon, L. D. Shvartsman, and B. Laikhtman, *Proceedings of the 24th International Conference on The Physics of Semiconductors (ICPS-24)*, Jerusalem, Israel, edited by D. Gershoni (World Scientific, Singapore, 1999).

[15] P. Voisin, G. Bastard, and M. Voos, Phys. Rev. B **29**, 935 (1984).

[16] A. J. L. Poulter, M. Lakrimi, R. J. Nicholas, N. J. Mason, and P. J. Walker, Phys. Rev. B **59**, 10 785 (1999).

[17] E. O. Kane, in *Handbook on Semiconductors*, edited by T. S. Moss (North-Holland Amsterdam, 1982), p. 193.

[18] A. M. Cohen and G. E. Marques, Phys. Rev. B **41**, 10 608 (1990).

[19] T. A. Vaughan, Ph.D. thesis, Oxford, 1995.

[20] R. W. Martin, M. Lakrimi, S. K. Haywood, R. J. Nicholas, N. J. Mason, and P. J. Walker, in *High Magnetic Fields in Semiconductor Physics III*, Springer Series in Solid-State Sciences, Vol. 101 (Springer, Berlin, 1992), p. 420.